

Peroxule extension over ER-defined paths constitutes a rapid subcellular response to hydroxyl stress

Alison M. Sinclair, Chris P. Trobacher, Neeta Mathur, John S. Greenwood and Jaideep Mathur*

Department of Molecular and Cellular Biology, University of Guelph, Guelph, ON, Canada

Received 5 January 2009; revised 17 February 2009; accepted 27 February 2009; published online 7 April 2009.

*For correspondence (fax +1 519 837 1802; e-mail jmathur@uoguelph.ca).

SUMMARY

Plants survive against myriad environmental odds while remaining rooted to a single spot. The time scale over which plant cells can respond to environmental cues is seldom appreciated. Fluorescent protein-assisted live imaging of peroxisomes reveals that they respond within seconds of exposure to hydrogen peroxide and hydroxyl radicals by producing dynamic extensions called peroxules. Observations of the *Arabidopsis flu* mutant and treatments with xenobiotics eliciting singlet oxygen and superoxide reactive oxygen species suggest that the observed responses are specific for hydroxyl radicals. Prolonged exposure to hydroxyl radicals inhibits peroxule extension, and instead causes motile and spherical peroxisomes in a cell to become immotile and elongate several-fold. Expression of photo-convertible EosFP-PTS1 demonstrates that vermiform peroxisomes result from rapid stretching of individual peroxisomes, while the subsequent 'beads-on-a-string' morphology results from differential protein distribution within an elongated tubule. Over time, the beads in elongated peroxisomes also extend peroxules randomly before undergoing asynchronous, asymmetrical fission. Peroxule extension does not appear to involve cytoskeletal elements directly, but is closely aligned with and reflects the dynamics of ER tubules. Peroxisomal responses reveal a rapidly invoked subcellular machinery that is involved in recognition of hydroxyl stress thresholds, and its possible remediation locally through extension of peroxules or globally by increasing peroxisome numbers. A matrix protein retro-flow mechanism that supports peroxisome–ER connectivity in plant cells is suggested.

Keywords: EosFP, endoplasmic reticulum, *flu* mutant, peroxisomes, peroxules, reactive oxygen species.

INTRODUCTION

Interpretation of environmental cues and the triggering of appropriate cellular responses while remaining rooted to a single place are essential for plant survival. Despite acknowledging plant sensitivity to the environment and significant advances in uncovering molecular cascades involved in plant growth and development, our understanding of the rapidity with which a plant cell might respond to cues is still rudimentary. Consequently, most approaches aimed at understanding plant cell responses to stress employ regimes that extend over hours and days, and thus our understanding of plant responses is very different from the plant cell's perception of a stimulus. We postulated that the plant cell must be able to respond very rapidly to changes in its environment in order to minimize subcellular damage. Further, specific stresses may range from moderate to very severe. Similarly, a stress might affect only a small region of the cell or involve the entire cell. The plant's response machinery must be able to distinguish between these parameters and react appropriately. The use of fluo-

rescent proteins targeted to numerous subcellular structures has significantly increased our ability to observe and understand organelle dynamics and interactions in living plant cells (Mathur, 2007).

Here we have used peroxisomes, which are ubiquitous eukaryotic organelles, in a proof-of-concept study aimed at establishing how quickly a plant cell responds to reactive oxygen species (ROS). Peroxisomes are best known for their role in production as well as scavenging of hydrogen peroxide (H₂O₂) (de Duve and Baudhuin, 1966). Although generally accepted as globular, single-membrane-bound vesicular organelles with diameters ranging from 0.2 to 1.5 µm, peroxisomes of various sizes and shapes ranging from elongate or tubular to reticulate have also been reported in various organisms (Schrader *et al.*, 1999, 2000; Cutler *et al.*, 2000; Mano *et al.*, 2002; Lingard and Trelease, 2006; Geuze *et al.*, 2007). Although early electron microscopy-based observations simply reported peroxisomes of various shapes (Frederick *et al.*, 1968), use of fluorescent

protein tags has facilitated an appreciation of the rapidity of peroxisome pleiomorphy in living cells. Thus, Cutler *et al.* (2000) described the dynamics of tubular extensions from torus-like organelles, subsequently identified by them as peroxisomes. Mano *et al.* (2002) and Jedd and Chua (2002) reported similar extensions by GFP-assisted live imaging of peroxisomes. Recently, in a review that compared morphologically similar structures such as plastid stromules (reviewed by Hanson and Sattarzadeh, 2008) and mitochondrial matrixules (reviewed by Logan, 2006), peroxisomal extensions were named 'peroxules' (Scott *et al.*, 2007). Scott *et al.* further suggest that studies of plants with mutations of dynamin-related proteins 3A (Mano *et al.*, 2004) and 3B (Zhang and Hu, 2009), which show similar peroxisomal phenotypes, may provide an understanding of the molecular basis for peroxisomal formation. However, the causal factors behind peroxule extension, the time required for response elicitation, and its consequences and implications for the cell have not been elucidated so far. We reasoned that understanding the spatio-temporal aspects of pleiomorphy in ROS-scavenging peroxisomes might provide additional information about the plant cell's stress-responsive machinery.

As part of our strategy to observe rapid subcellular responses of plants, the time scale for observations in these studies was reduced to a maximum of 2 h. An early subcellular response was defined as that occurring between 10 and 120 sec, and a late response was defined as that observed between 2 min and 2 h. It was reasoned that these short time frames would allow more accurate cause-and-effect correlations to be established.

RESULTS AND DISCUSSION

Peroxule extension is a common transient phenomenon in plant cells

Peroxisomes were visualized in living cells of transgenic *Arabidopsis* lines carrying yellow fluorescent protein (YFP) fused to a tripeptide (SKL) peroxisome-targeting signal (YFP-PTS1; Mathur *et al.*, 2002). Observations on 25–35 μm long hypocotyl cells of 10-day-old YFP-PTS1 seedlings revealed between 60 and 130 motile, globular peroxisomes per cell, with diameters ranging from 0.8 to 1.2 μm ($n = 120$). Sporadically, between 15 and 35 peroxisomes in any randomly chosen hypocotyl cell showed thin (450 ± 50 nm diameter) tubular protrusions extending up to 5–7 μm from their surface ($n = 100$ cells) (Figure 1a). These protrusions matched the morphology-based definition of peroxules suggested by Scott *et al.* (2007). No correlation was found between the position of a peroxule extension from a peroxisome and the direction of cytoplasmic streaming in a cell. Thus, based on the direction of movement of peroxisomes, the peroxules could be considered leading or trailing. In some cases, a peroxisome appeared in the middle, with

peroxules extending on both sides. Alternatively, in cotyledon pavement cells, peroxisomes, which were often found lodged between chloroplasts, routinely showed extending and retracting peroxules. These appeared to probe the region around a chloroplast in a waving movement (Figure 1a), extend over the curved chloroplast surface (Figure 1b), or connect with several other peroxisomes to form a complete ring around the chloroplast (Figure 1c). A single peroxisome located between several chloroplasts may simultaneously extend multiple tubules of unequal length in various directions for transient contacts. In contrast to aerial tissue, peroxule extension was seen infrequently in root cells. However, peroxisomes in root epidermal cells were generally elongated (1.6 ± 0.3 μm long; 0.6 ± 0.2 μm wide; $n = 120$) compared to the more iso-diametric forms in green tissue. Senescing cotyledon cells ($n = 20$ cells from 10 cotyledons) contained a mixture of immotile elongated peroxisomes that show Brownian oscillation (25.6%) and motile potentially peroxule-extending spherical peroxisomes (74.3%) (Figure S1).

Based on the above observations, it was concluded that, even within unstressed seedlings, peroxisome morphology ranges from spherical to slightly elongate. Peroxules occurred as transient extensions and were more common in chloroplast-containing cells compared with achlorophyllous cells. The extension of peroxules from peroxisomes, which are well-established ROS emitting and scavenging organelles (de Duve and Baudhuin, 1966), their transient nature and their probing action around chloroplasts suggested that peroxule formation could be a response to reactive oxygen. This hypothesis was tested through further experiments.

Peroxule extension occurs in response to low levels of hydroxyl radical ROS

Many kinds of reactive oxygen species (ROS), including non-radical singlet oxygen ($^1\text{O}_2^*$) and H_2O_2 , superoxide (O_2^-), and hydroxyl radical ($\text{HO}\cdot$), are produced during light-induced oxidative stress in chlorophyllous cells (Halliwell and Gutteridge, 1984; Magder, 2006). Various hypolipidemic drugs and herbicides (Harris and Knox, 1972; Palma *et al.*, 1991), as well as UV irradiation and H_2O_2 treatments [Palma *et al.*, 1991 (plants); Schrader *et al.*, 1999 (animal cells)], have been shown to change peroxisome morphology and lead to their proliferation. Many ROS trigger secondary ROS formation (op den Camp *et al.*, 2003; Magder, 2006), making it difficult to pin down a direct cause-and-effect relationship. A critical evaluation of previous studies involving ROS treatments revealed that the time scale in these studies had been of the order of hours and days. Given the transient nature of peroxule extension, the results of long-term treatments and extended observations could prove to be misleading. Therefore, in our assessment of ROS-inducing chemicals and irradiation treatments, we focused on per-

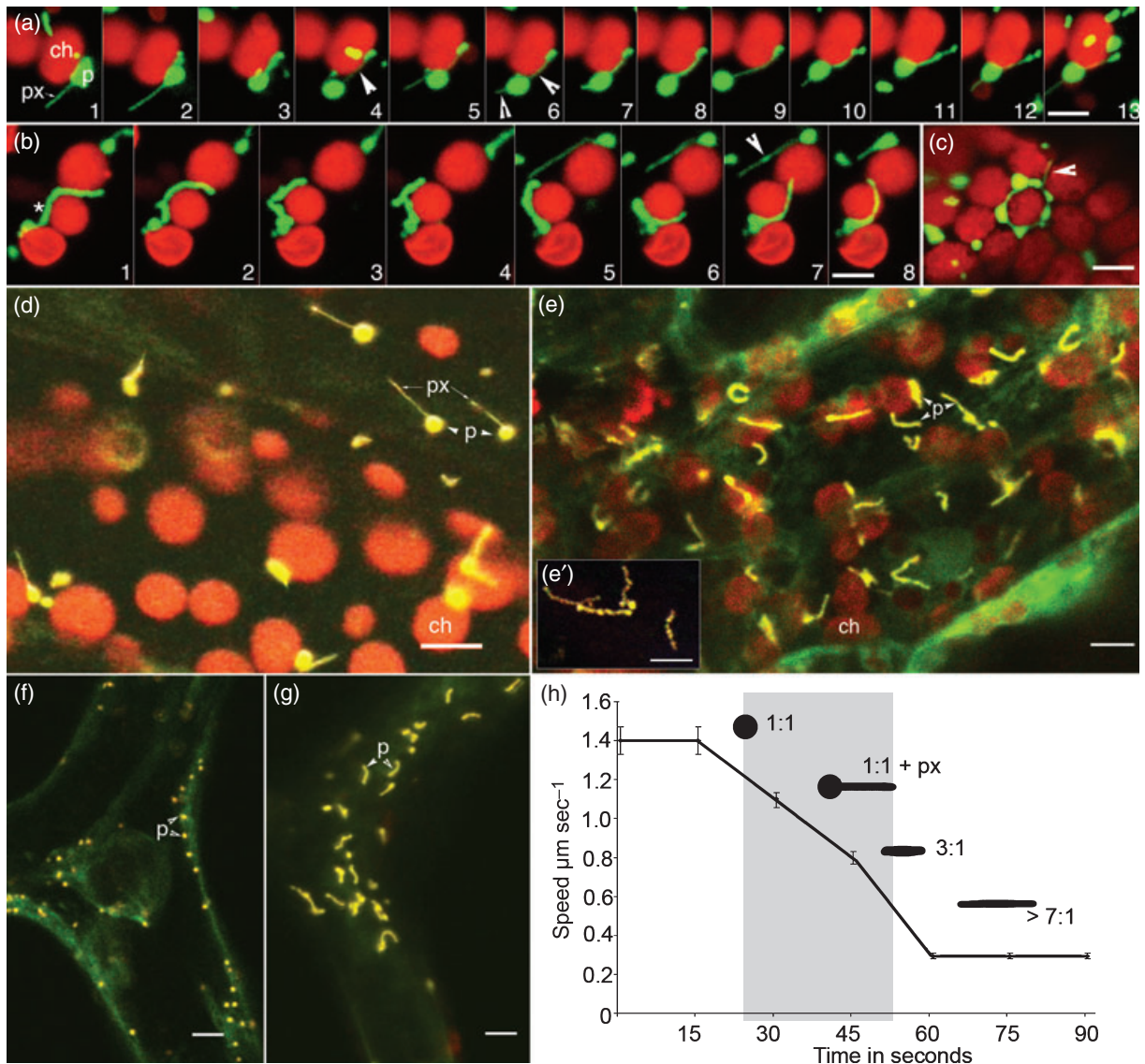


Figure 1. Peroxule extension as seen in cotyledon cells and in response to H_2O_2 and UV treatments in light-grown *Arabidopsis* plants expressing a YFP-PTS1 transgene.

(a) A single peroxisome (p) located near a chloroplast (ch) extends (frames 1, 2, 4, 7–13) and retracts (frames 3, 5, 6) a thin peroxule (px). In frames 4–6 (arrowheads), peroxules extend between two peroxisomes of different sizes, whereas frames 10–13 suggest a beaded peroxule. Total time lapse 42 sec (Movie S1).

(b) A single elongated peroxisome (*) curves around a chloroplast between frames 1 and 8, and a spherical peroxisome in the upper right-hand corner extends (frame 5) and retracts (frames 6–8) a peroxule. Note the transient beaded appearance of the peroxule that emerges in frame 6, which becomes pronounced in frame 7 (arrowhead) before disappearing (frame 8). Total time lapse 26 sec.

(c) A single chloroplast encircled by peroxisomes connected to each other by peroxules. An extension (arrowhead) reaches out towards a neighboring chloroplast. (d–g) Rapid peroxisome elongation seen in response to hydroxyl radicals created after H_2O_2 and UV stress. Note that the length of peroxules, such as in (d), often exceeds that of fully elongated peroxisomes. However, the tubule diameter is similar for both.

(d) Hypocotyl cell showing extensive peroxule (px) formation upon treatment with 0.08 M H_2O_2 solution for 120 sec. Note that peroxisomes (p) still maintain an approximately 1.2 μm diameter spherical form while extending peroxules that are 200–400 nm in diameter and 5–7 μm long.

(e) Hypocotyl cells showing 3–6 μm long, arrested peroxisomes (p) upon exposure to 0.8 M H_2O_2 solution for 60 sec. The inset (e') shows the beaded appearance of elongated peroxisomes during a recovery phase of approximately 15 min after the H_2O_2 treatment.

(f) A trichome cell with spherical peroxisomes before exposure to UV.

(g) The same cell with elongated peroxisomes following UV exposure for 90 sec.

(h) Effect of progressively increasing UV exposure time on peroxisome motility and morphology. Both shape and motility changes become apparent after between 25 and 45 sec of exposure. Peroxisomes that were allowed to recover from this exposure produced peroxules, whereas those subjected to a longer exposure of 60–90 sec show elongated tubules with length:width ratios ranging from 3:1 to 7:1. Note that peroxisomes appear to become narrower and show tubule diameters similar to those of peroxules.

Scale bar = 5 μm .

oxule formation within the shortest time after treatment. Peroxisomes are renowned for their H₂O₂-scavenging capabilities, and therefore this ROS was investigated first.

YFP-PTS1 seedlings that were 6–8 days old were exposed to 0.008, 0.08 or 0.8 M (corresponding to approximately 0.03 to 3%) concentrations of H₂O₂ for up to 120 sec, washed for 60 sec in distilled water, and observed over 5 min. Peroxisomes maintained their normal motility (approximately 1.4 ± 0.5 μm sec⁻¹; *n* = 150) and spherical shape (length:width ratio = 1:1) in the 0.008 and 0.08 M solutions. In the 0.8 M solution, peroxisome motility decreased to 0.8 ± 0.3 μm sec⁻¹ (*n* = 100) within 45 sec of treatment, while the number of peroxisomes with extensions of up to 10 μm increased by nearly fourfold compared to untreated controls (Figure 1d). Prolonging the exposure to 0.8 M H₂O₂ solution to 120 sec caused all peroxisomes to become nearly non-motile (0.3 ± 0.1 μm sec⁻¹; *n* = 250), limited their range of movements to small, and stretch into 3–5 μm long tubules (average length:width ratio 3:1; Figure 1e). Occasional tubule lengths of up to 8 μm were observed. A similar effect was achieved in 0.08 M solution over 15 min. H₂O₂ is a non-radical ROS, and its breakdown results in the even more toxic hydroxyl radicals (Magder, 2006). ROS specificity was thus achieved by establishing a Fenton reaction using a copper chloride/ascorbate mixture that generates hydroxyl radicals (Foreman *et al.*, 2003). Exposure to the reagent for 60–120 sec predominantly resulted in elongated peroxisomes. However, treatment for longer than 5 min resulted in loss of peroxisomal definition and a diffuse fluorescence in the cell, suggesting irrevocable damage to cell membranes. Washing the CuCl₂/ascorbate solutions within 1 min allowed cells to maintain brightly fluorescent elongated peroxisomes. Although they were immotile immediately following the treatment, tubular peroxisomes progressively developed a beaded appearance and regained complete motility over 2 h.

Another treatment that gives rise to hydroxyl radicals is UV irradiation of living cells (Taira *et al.*, 1992; Frohnmeyer and Staiger 2003). Individual hypocotyl cells in YFP-PTS1 seedlings were focused upon using a 40× lens and exposed to 390 ± 50 nm UV-A for 15–90 sec (Figure 1f–h). By 90 sec, nearly all peroxisomes had acquired an elongated shape, with lengths ranging between 3 and 5 μm (*n* = 100; Figure 1f versus Figure 1g). The first signs of a change in peroxisome behavior were observed between 25 and 45 sec after irradiation of individual cells (Figure 1h). Long distance motility of peroxisomes occurring over 20–40 μm was reduced to movements limited within 5–10 μm, and their velocity slowed to a barely perceptible 0.3 ± 0.05 μm sec⁻¹ (*n* = 100). In contrast to H₂O₂ and CuCl₂/ascorbate treatment, UV irradiation was performed on single cells. This illumination strategy created a peripheral zone around the focused beam where cells received a lower UV exposure. Spherical peroxisomes in these cells were motile and extended

5–8 μm peroxules. Interestingly, the diameters of tubular peroxisomes and peroxules were found to be similar.

Although clear differences exist between UV and H₂O₂ treatments, both result in similar ROS. Thus the experiments reinforce the notion of similar response elicitation, and enabled us to conclude that low levels of hydroxyl ROS are responsible for peroxule extension from regions of a peroxisome, whereas a higher dosage of the same ROS leads to tubulation of peroxisomes. The response of peroxisomes to other ROS was assessed further in an Arabidopsis mutant that produces excessive singlet oxygen, and by treating YFP-PTS1 plants with chemicals inducing singlet and superoxide ROS.

Singlet oxygen and superoxide ROS do not evoke peroxule extension or peroxisome elongation

The conditional *flu* mutant of Arabidopsis is blocked in the negative feedback loop that abolishes chlorophyll biosynthesis in the dark (Meskauskiene *et al.*, 2001). Consequently, dark-grown *flu* plants accumulate the photo-sensitizer protochlorophyllide (Pchl_{id}) that creates singlet oxygen upon illumination (op den Camp *et al.*, 2003). High amounts of singlet oxygen are released within the plastid compartment in *flu* cells within 5 min of illumination and lead to rapid photo-bleaching (Figure 2a versus Figure 2b). In our hands, signs of cellular breakdown in the form of breaking chloroplasts appeared within minutes of exposure, and small lesions and discolorations became visible within 2 h. However, YFP-PTS1-highlighted peroxisomes in *flu* cells (25 seedlings, >500 individual cells) were observed to move at normal velocities ranging from 0.7 to 2.8 μm sec⁻¹ without any change in their spherical morphology even after being illuminated for 2 h (Figure 2c). These peroxisomes did not extend peroxules. Observations at 30 min intervals over an 8 h period showed that cells in the lower hypocotyl showed normal peroxisomal shape and motility. However, by this time, *flu* cotyledons showed pronounced bleaching in comparison to wild-type. Peroxisomes in photo-damaged cells were frequently clumped (Figure 2d), and less fluorescent but still spherical. Occasionally, slightly elongated (length:width ratio 2.2:1) dumbbell-shaped peroxisomes were observed in bleached cells. Treatment of YFP-PTS1 seedlings with a singlet oxygen-inducing xanthine/xanthine oxidase mixture for up to 2 h confirmed the non-responsiveness of peroxisomes to singlet oxygen. It was concluded that singlet oxygen is not directly responsible for rapid peroxule extension or peroxisome elongation.

To further assess the specificity of the response to hydroxyl radicals, dark-grown *flu* seedlings were checked first for the presence of motile, spherical peroxisomes before exposing them to 0.8 M H₂O₂ for 30 sec. Peroxules (Figure 2e) and tubular peroxisomes (Figure 2f) formed in *flu* cells within 2 min after treatment. The peroxisomes in *flu* are thus competent to respond to hydroxyl radicals.

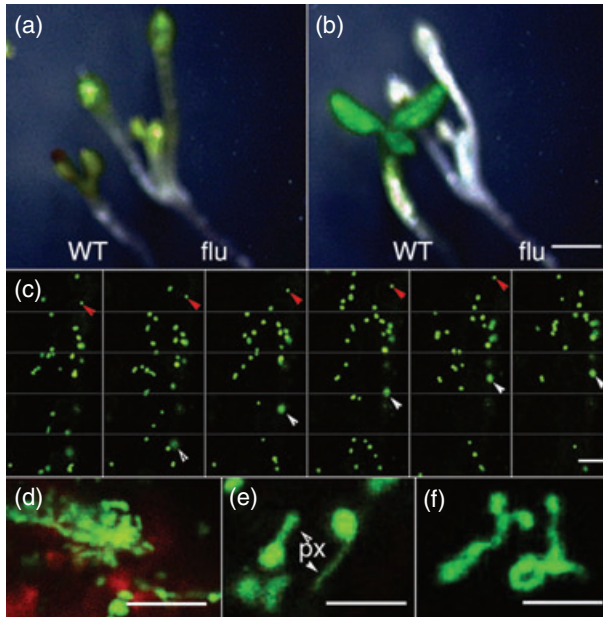


Figure 2. Peroxisome response in the excess singlet oxygen-generating *flu* mutant of *Arabidopsis thaliana*.

(a) Seven-day-old dark grown wild-type and *flu* mutant seedlings exposed to light for 5 min.

(b) Seedlings shown in (a) after 32 h. Note that whereas the wild-type (WT) seedling has greened and opened its first pair of leaves, the *flu* mutant has bleached. The earliest signs of bleaching appear within 2 h.

(c) Representative time lapse images showing unchanged peroxisome motility and morphology in *flu* plants exposed to light for 2 h. Similar peroxisomal behavior is maintained even after 8 h of exposure.

(d) Diffuse clusters of peroxisomes observed in cotyledon and hypocotyl hook after 8 h of exposure.

(e, f) Exposure to 0.8 M H_2O_2 for 30 sec resulted in (e) a few peroxules (px) and (f) elongated peroxisomes.

Spraying and dipping treatments performed for 2 h in the light using 10 μ M solutions of superoxide radical elicitors such as isoproturon, rose bengal, paraquat and clofibrate did not alter the peroxisome morphology either. These chemicals have been used as ROS inducers in physiological and biochemical studies aimed at understanding stress mechanisms (Halliwell and Gutteridge, 1984; Palma *et al.*, 1991). The concentrations used were frequently higher, and the treatments were relatively harsh and involved explanted tissue. The other major difference was the considerably longer time scale for observations compared to this study. Nevertheless, peroxisomes in seedlings submerged for more than 2 h in the various xenobiotic solutions as well as distilled water controls frequently showed reduced motility and increased size ($2.5 \pm 0.8 \mu$ m diameter). This general response was attributed to hypoxia.

Based on the above experiments, it was concluded that both peroxule formation and the elongation of a peroxisome into a narrow tubule are responses that are specific to hydroxyl radical stress. One possible explanation for these observations might lie in the biochemical lipid peroxidation

activity attributed to a toxic $HO\cdot$ radical as it extracts an H from a methylene (CH_2) to create the reactive $\cdot CH$ radical (Stoys and Bagchi, 1995; Finkel and Holbrook, 2000). This carbon radical then attacks other CH_2 groups in lipid molecules, and alters the fluidity and shape of lipid-containing membranes through a chain reaction (Magder, 2006). Peroxisomal elongation might also be seen at late time points in other ROS treatments as a secondary response, as the formation of toxic hydroxyl radicals can be induced through cross-talk between various reactive molecules.

It is noteworthy that peroxisomes that extend peroxules invariably maintained their approximately 1 μ m iso-diametric form, whereas the tubulated peroxisomes created in response to high stress did not revert directly to single spheres. Instead tubules became beaded. Although peroxisome elongation followed by fission has often been presented as a logical sequence of events leading to peroxisome proliferation (Thoms and Erdmann, 2005; Fagarasanu *et al.*, 2006; Tabak *et al.*, 2006; Titorenko and Mullen, 2006), actual visualization of peroxisome fission has not been accomplished in any organism and was therefore investigated further.

Tubular beaded peroxisomes extend peroxules before fission

Both peroxules (Figure 1b, panel 7) and tubular peroxisomes in their late stages show 'beadiness' (inset Figure 1e'). Whereas in the more dynamic peroxules, a bead can appear anywhere within the extension and be rapidly retracted into the main peroxisomal body (Figure 1a,b), 'beadiness' in immotile vermiform peroxisomes only appears progressively. The appearance of beads suggested that matrix proteins could be differentially distributed within a tubule. This was analyzed by fluorescence intensity profiling of individual elongated peroxisomes (Figure 3a,b). Based on the higher fluorescence intensity of the YFP-PTS1 signal, the beads were confirmed as regions of higher protein concentration than the neighboring areas (Figure 3a,b). Subsequent observations of beaded peroxisomes used dynamic fluorescent intensity mapping by splitting the total fluorescence in a confocal scanned image equally into red, green and blue (RGB) colors, with blue denoting the highest levels of fluorescence. This revealed that neither the position of the beads nor their numbers remained constant over time. The dynamics of elongated peroxisomes involved a progressive increase in their wriggling motion (Figure 3c), often accompanied by the random extension of peroxules from beads (Figure 3c). Increased motility often allowed beaded peroxisomes to interact and form clumps (Figure 3). Peroxisome motility continued to increase until by 60 min most peroxisomes had extended peroxules and were moving at rates of $0.8 \pm 0.3 \mu$ m sec^{-1} . Although internal rearrangements were a constant feature in individual tubules, actual fission was not observed until peroxisomes were completely

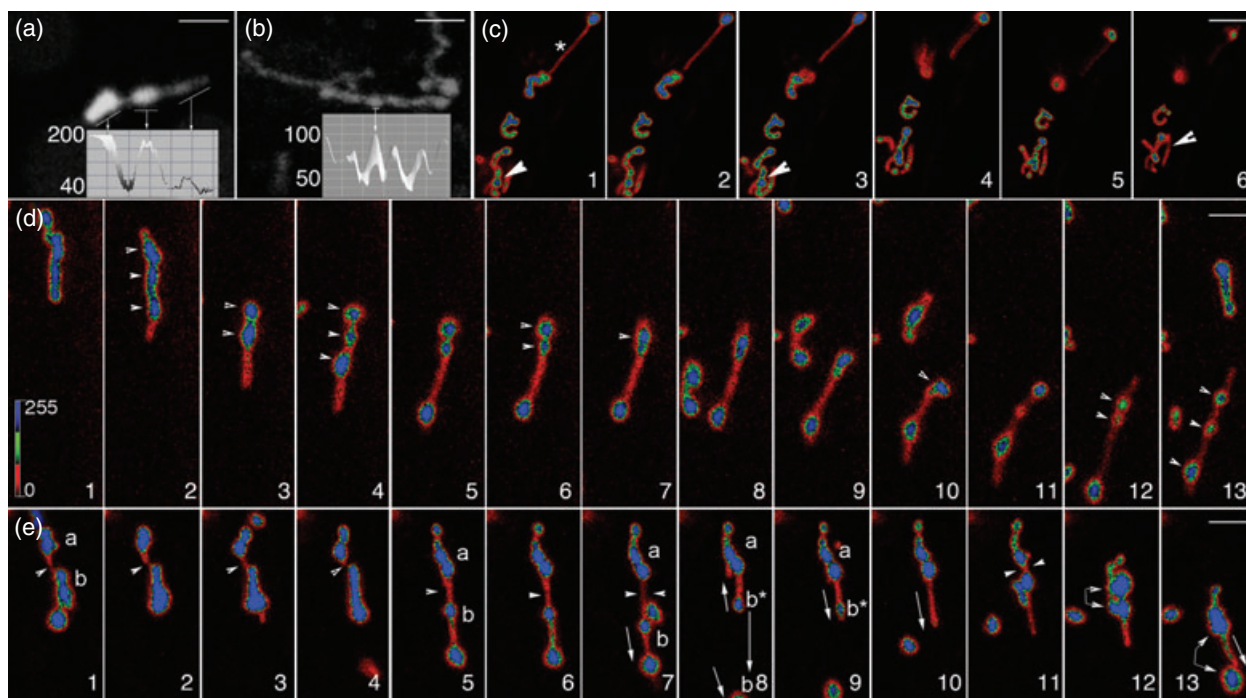


Figure 3. The dynamics of beaded peroxisomes and their fission.

(a, b) Fluorescence intensity measurements of (a) a peroxule and (b) an elongated beaded peroxisome show fluorescent peaks coinciding with beads. Neighboring areas show lower fluorescence values, suggesting that the distribution of YFP-PTS1 matrix protein varies within the tubules.

(c) Six time-lapse frames each separated by 6 sec show the wriggling motion of peroxisomal clumps. The images were acquired using real-time fluorescence intensity mapping based on color partitioning software P.Color5 LUT and show peroxisomal dynamics between 20 and 45 min after treatment with 0.8 M H₂O₂ for 30 sec. An RGB color bar is shown in panel 1 of (d). Blue indicates the part with the most intense fluorescence and red with the least. A peroxule (*) is extended and connects with a beaded peroxisome before retracting (frames 2–6). The lower portion of each panel shows the morphing of a clump, and shows beaded and non-beaded regions (arrowheads in panels 1 and 3) as they change positions within the tubule.

(d) Changes in the distribution of matrix protein within a single tubule over approximately 75 sec, showing the rapidity of changes within a tubule (arrowheads indicate beads) that convert it from a smooth (panel 1) into a progressively beaded form (panels 2–6). The internal re-organization suggests merging of beads (panel 7 compared to panel 6), changes in the distance between beads (panels 7–10), and their reappearance as discrete foci. Note that individual snapshots from this sequence suggest separate stages of elongation and bead formation in peroxisomes.

(e) Time-lapse sequence over approximately 75 sec showing fission of a beaded peroxisome by a tearing-apart mechanism. Panels 1–4 show a thin neck (arrowheads) between two portions of a peroxisome designated 'a' and 'b'. The neck region stretches in panel 5 and becomes tenuous in panel 7 (arrowheads). Fission occurs in panel 8 as the 'b' region breaks off, leaving 'b*' still attached to 'a'. Peroxule extension starts again in panel 10, and narrowing starts to occur in panel 11, followed by progressive stretching between panels 12 and 13 (arrowheads).

motile. Fission of beaded tubules was asynchronous, and as part of a tubule broke off and moved in one direction, the remaining portion usually snapped back in the other direction. This type of fission suggested that peroxisomes were being torn apart. This observation was supported by the inequality of the fission, with regions carrying with them one or more 'beads' of high protein concentration. Once initiated, the break-up of elongated peroxisomes was rapid and generally lasted only a few minutes. By the end of 2 h, hardly any elongated peroxisomes could be observed in the cells.

These observations raised a question regarding the nature of the tubular peroxisomes, and whether, as suggested by Mano *et al.* (2002), they could have been created through the fusion of one or more individual peroxisomes in close proximity. If such fusion had taken place, then the observed fission of peroxisomes could simply reflect their re-separation upon removal of stress. As this was difficult to prove in peroxisomes highlighted using a single colored

fluorescent protein, a novel strategy employing a photo-convertible protein was used.

Eos-SKL reveals peroxisome tubulation resulting from rapid expansion of a single peroxisomal domain

EosFP is a green → red photo-convertible protein (Wiedenmann *et al.*, 2004). The C-terminus of a monomeric EosFP was modified to code for the tri-peptide SKL, which allowed its successful targeting to peroxisomes. All peroxisomes in a cell transiently expressing Eos-PTS1 were highlighted in green. Local photo-conversion of a sub-population of peroxisomes in the cell by 15 sec exposure to 400 nm centered wavelength resulted in a mix of red, green and partially converted yellow peroxisomes (Figure 4a). The cell with the mixture of differently colored peroxisomes was exposed indirectly to ROS by UV-irradiating a neighboring chloroplast-containing cell for 120 sec while taking care to shield the photo-converted cell from additional exposure. It was

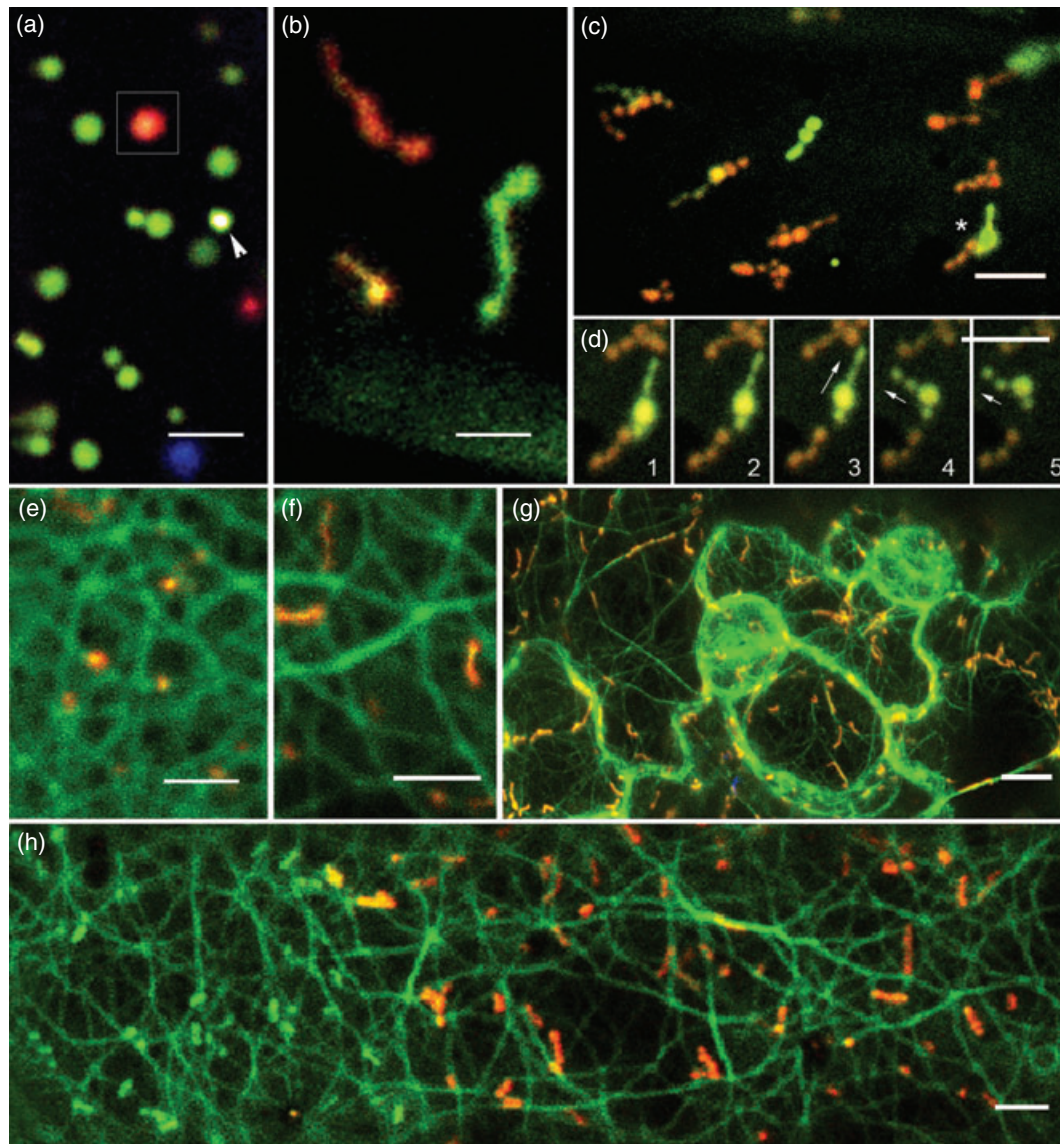


Figure 4. EosFP-SKL-assisted determination of peroxisome elongation, and co-visualization of YFP-PTS1-labeled peroxisomes with GFP-mTalin-labeled F-actin. (a) Peroxisomes highlighted using EosFP-SKL. The image shows a single red peroxisome (boxed) in which EosFP has been photo-converted, and a peroxisome in which it has been partially converted and appears yellow-green (arrowhead). Unconverted peroxisomes appear green. (b) Exposure of a cell as shown in (a) to 0.8 M H₂O₂ for 30 sec results in single peroxisome-derived red, green and yellow elongated peroxisomes. (c,d) EosFP-SKL-targeted peroxisomes of various colors show a beaded phenotype. (c) Some peroxisomes '*' give the appearance of having fused. However, time-lapse imaging of two red and green beaded peroxisomes over 2 min showed their separation while maintaining their identities (d). Arrows in panels 3–5 show the direction of movement followed by a green beaded peroxisome (Movie S2). (e, f) Spherical YFP-PTS1-labeled peroxisomes co-visualized with GFP-mTalin, which highlights F-actin. In (f), the same cell as in (e) has been exposed to 0.8 M H₂O₂ for 30 sec, resulting in elongated peroxisomes. The F-actin appears unchanged. (g) Fine F-actin highlighted using GFP-mTalin does not break down upon exposure to UV for 45 sec. However, peroxisomes elongate and lie along actin filaments. (h) A compressed stack of 10 images through a cell transiently expressing GFP-mTalin and EosFP-PTS1 and partially exposed to approximately 400 nm centered wavelengths for 60 sec. Elongated red photo-converted and green non-converted peroxisomes are seen. The actin cytoskeleton in the UV-illuminated region appears very similar throughout the cell. The gap in the middle of the image is an artifact that denotes the uppermost limit of the z-stack. Green peroxisomes appear fuzzy, as they were more motile during imaging compared to the nearly immobilized elongated red peroxisomes. Scale bars = 2.5 μm (a,b) and 5 μm (c–h).

expected that, if peroxisomes fuse with each other, a combination of green–red, yellow–green and yellow–red elongated structures would be observed. Alternatively, if the elongated morphology resulted from a single peroxisome, a

single color would be seen. Images of peroxisomes acquired 5 min after their exposure to indirect ROS showed individual, immotile, elongated red, green and yellow peroxisomes with a beaded appearance (Figure 4b). The observations

were confirmed by exposing photo-converted peroxisomes to 0.8 M H₂O₂ for 30 sec. Around 30 min after the H₂O₂ treatment, several beaded peroxisomes of red and green color were observed in juxtaposition (Figure 4c). In some cases, this suggested fusion of elongated peroxisomes (Figure 4c, marked by an asterisk). However, observations over 10 min showed beaded peroxisomes of different colors separating from aggregates and moving in different directions (Figure 4d, panels 1–5).

The observations clearly show rapid stretching of the peroxisomal domain into a several-fold elongated structure, and its subsequent reorganization into normal-sized peroxisomes over time. The elongation of a single peroxisome differed from the local extension of a peroxule in its consequences. Whereas peroxules are extended and retracted rapidly from a peroxisome and can sometimes get broken off, the elongated peroxisomes shows a clear 'beadiness', suggestive of additional peroxisomes being created within the tubule. Subsequent fission of the elongated beaded peroxisome has been shown to result in an increased number of peroxisomes (Lingard and Trelease, 2006), and is considered an essential component of the peroxisomal life cycle (Thoms and Erdmann, 2005; Fagarsanu *et al.*, 2006). More importantly, the observations demonstrate the cell's ability to discriminate between transient responses needed for localized ROS scavenging versus a more global response to strong stress requiring an increase in peroxisomal numbers.

As shown here, both peroxule formation and peroxisome tubulation are rapidly elicited responses. Moreover, pleomorphic peroxules extend and retract while moving and probing subcellular regions. Peroxisomes in plants are known to move along F-actin tracks in a myosin-dependent manner (Jedd and Chua, 2002; Mano *et al.*, 2002; Mathur *et al.*, 2002). Further investigations thus involved seeking correlations between the dynamic alterations in peroxisome morphology and cytoskeletal elements.

Neither peroxule extension nor peroxisome elongation involve major alterations in the cytoskeleton

Transgenic Arabidopsis lines carrying YFP-PTS1 and a GFP::mTalin probe to highlight peroxisomes and filamentous actin simultaneously were exposed to UV and H₂O₂. Peroxule formation was observed when mild treatments were used, whereas harsher treatments arrested and elongated peroxisomes (Figure 4e–g). Although elongated peroxisomes aligned themselves along considerable lengths of intact actin filaments (Figure 4f,g), no rapid changes in F-actin strands or a breakdown in their organization were observed to explain the dynamic behavior of peroxules. An additional experiment was performed using EosFP-PTS1 and GFP::mTalin. Exposure of a region of the cell to UV for 60 sec led to both photo-conversion and elongation of EosFP-PTS1-labeled peroxisomes (Figure 4h, right-hand side).

The unexposed region of the cell contained small nearly spherical green peroxisomes, some of which had short peroxules. No changes were apparent in the F-actin mesh (Figure 4h). Although peroxisome motility in plants is actin/myosin-dependent (Jedd and Chua, 2002), it has been associated with microtubules and related motor proteins in animal cells (Schradler *et al.*, 1996). ROS-eliciting treatment of double transgenic YFP-PTS and GFP::mbdMAP4 plants that allow simultaneous visualization of peroxisomes and microtubules showed peroxules and elongated peroxisomes but no changes in cortical microtubule arrays that could explain peroxule dynamics (data not shown).

As observations of peroxisomes and cytoskeletal elements did not provide a clear explanation for the rapid shape change and dynamics of peroxules, further investigations focused on the endoplasmic reticulum (ER), which constitutes another dynamic actin/myosin-dependent system in the cell.

Peroxules extend along paths defined by ER tubules

Transgenic plants of Arabidopsis carrying YFP-PTS1 and RFP-HDEL were generated for the simultaneous visualization of peroxisomes and the ER. Hypocotyl cells with peroxisomes in the vicinity of chloroplasts were focused upon using an epi-fluorescent microscope. Peroxule extension was elicited by UV-irradiating 3–5 chloroplasts for approximately 45 sec (Figure 5). Within 1 min, peroxules could be observed near these chloroplasts. Peroxules possessed nearly similar diameters as RFP-HDEL-highlighted ER tubules (300–500 nm) and extended along ER polygons (Figure 5a, panels 1–12). In a separate experiment, seedlings were exposed to 0.4 M H₂O₂ for 3 min, and this resulted in elongated peroxisomes in a few cells. Time-lapse imaging of an elongated peroxisome (Figure 5b, panels 1–7) 1 h after the treatment clearly showed that its dynamics followed those of underlying ER tubules. In cells where the ER showed low motility, peroxisomes of various sizes lay along ER tubules but showed only Brownian oscillations. Further, treatment of cells with motile elongated peroxisomes and ER using 2,3-butanedione monoxime, a specific inhibitor of myosin ATPase (Herrmann *et al.*, 1992), resulted in cessation of motility for both organelles (data not shown). On the basis of these observations, it was concluded that peroxule dimensions and dynamics are very similar to those of contiguous ER tubules.

Although the precise mechanisms for the coincident behavior of peroxules and ER tubules are presently unclear, it is notable that early electron microscopic pictures of plant (Frederick *et al.*, 1968) and animal cells (Novikoff and Novikoff, 1972), as well as more recent electron tomography of peroxisomes from mouse dendritic cells (Geuze *et al.*, 2003), suggest peroxisome–ER connectivity. Further, a direct link between the endoplasmic reticulum and peroxisome biogenesis has been shown in fission yeast (Hoepfner *et al.*,

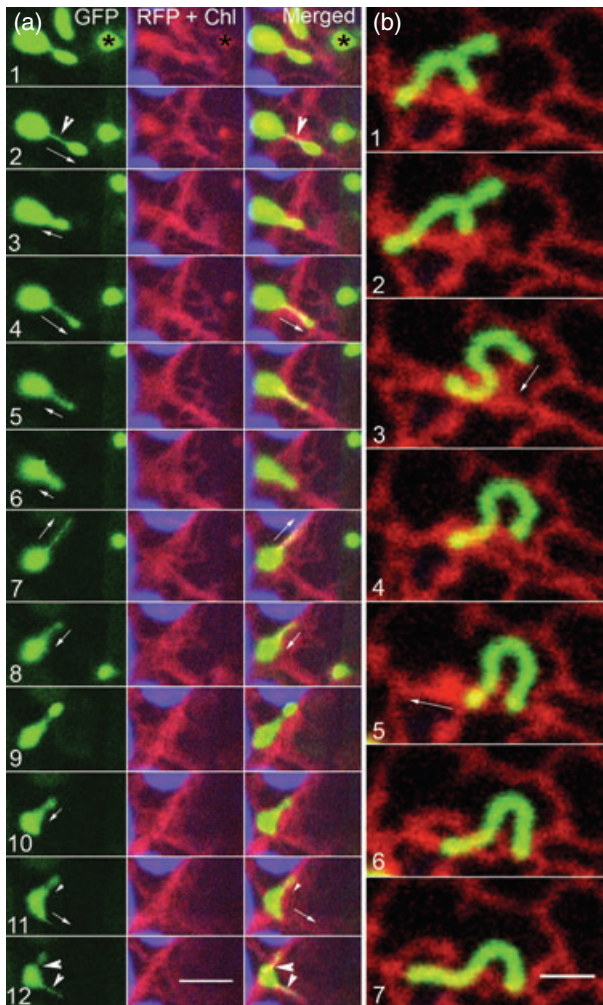


Figure 5. YFP-PTS1-labeled peroxules and an elongated peroxisome co-visualized with RFP-HDEL-labeled ER suggest their co-alignment.

(a) Images 1–12 of extending peroxules acquired over 3 min are sequential but the time lapse between them is not equal. Arrows in the GFP panels denote extension and retraction as well as changes in the direction of peroxules. The underlying red fluorescence of ER tubules in the middle and merged panels coincides with the path of peroxule extension. Chloroplasts have been false-colored blue, and the asterisk on the peroxisome (panel 1) provides a point of reference (Movie S3).

(b) The wriggling motion of an elongated peroxisome obtained after H_2O_2 treatment shown in seven snapshots from a time-lapse sequence clearly shows a correlation between ER tubules and peroxisome dynamics. Arrows in panels 3 and 5 indicate the ER tubule with which the peroxisome subsequently aligns (Movie S4).

Scale bars = 2.5 μm (a) and 5 μm (b).

2005; Kim *et al.*, 2006). In addition, both the ER and peroxisomes have been found to be dependent on actin and myosin machinery for their motility (Jedd and Chua, 2002; Reisen and Hanson, 2007). Nevertheless, current models of the peroxisome life cycle suggest that peroxisomes break off from the ER following their biogenesis (Fagarasanu *et al.*, 2006; Mullen and Trelease, 2006; Schrader and Fahimi, 2008). The observed alignment of tubular peroxules and elongated peroxisomes with ER

tubules, as well as their coincidental dynamic behavior, allow us to raise once again the possibility of the two organelles being connected. Interestingly, in studies on animal cells in which elongated peroxisomes have been observed, the ER has been speculated to be a ready source of membrane components (Purdue and Lazarow, 2001; Schrader and Fahimi, 2008). However, details on the mechanism for such exchange of membrane components are unclear. Neither has the rapidity of the peroxisomal response been taken into account in these studies. Now, in view of our findings, a mechanism that can account for both peroxule and vermiform peroxisome formation is suggested. This is based on ER–peroxisome connectivity, and involves retro-flow of peroxisome matrix proteins into contiguous ER tubules. Such protein retro-flow would clearly require the relaxation of mechanisms that maintain a peroxisomal domain in the ER. Thus it can be predicted that mutations in proteins possessing constrictase activity, such as dynamin-related proteins, would result in more peroxule-like behavior. This appears indeed to be the case in Arabidopsis DRP3A/3B mutants in which peroxule-extending peroxisomes similar to those described here have been reported (Mano *et al.*, 2004; Zhang and Hu, 2009). While the mechanism could be plant-specific, mutations in dynamin-related protein homologues in other organisms result in similar elongated peroxisomes (Koch *et al.*, 2003; reviewed by Thoms and Erdmann, 2005). Although the links are presently unclear, the retro-flow mechanism may involve peroxisome membrane proteins such as members of the peroxin 11 class, whose over-expression also leads to elongated peroxisomes (Lingard and Trelease, 2006; Orth *et al.*, 2007). Experiments designed to investigate further the retro-flow mechanism and peroxisome–ER continuity in plant cells are currently being performed.

CONCLUSIONS

The results presented here using peroxisomes as a stress-responsive organelle indicate the hitherto unappreciated rapidity of plant cell responsiveness to a specific but common oxidative stress. The temporal regime followed here was necessary to avoid confusing observations resulting from cross-talk between various ROS. The subcellular response time should thus be a major consideration in studies involving plant cells. In addition, this study provided an indication of cellular mechanics in response to stress thresholds. Peroxule extension might thus be interpreted as a local and transient response, ostensibly leading to stress alleviation; the formation of tubular peroxisomes and their subsequent break-up could signify an attempt by the cell to combat global stress by increasing the peroxisomal population. Finally, our live imaging-based observations lend strong support to conclusions reached in one of the earliest published observations on peroxisomes that suggested their close association with the ER (Novikoff and Novikoff, 1972).

EXPERIMENTAL PROCEDURES

Plant material, constructs and treatments

We used *Arabidopsis thaliana* (ecotype Landsberg *erecta*) plants carrying the YFP-PTS1 tag (Mathur *et al.*, 2002), GFP::mTalin (Kost *et al.*, 1998) or GFP::mbdMAP4 (Mathur and Chua, 2000) and the *Arabidopsis flu* mutant (op den Camp *et al.*, 2003) as described previously. The YFP-PTS1 tag was introduced into the *flu* background by crossing, and seeds from the third filial generation were used. The RFP-HDEL construct for the ER was created by swapping the GFP in mGPPER (Haseloff *et al.*, 1997) with a monomeric RFP (Campbell *et al.*, 2002), cloned into a pCAMBIA vector (<http://www.cambia.org.au>) under the control of a CaMV 35S promoter, and introduced into *Arabidopsis* plants using *Agrobacterium tumefaciens*. The monomeric EosFP-PTS1 construct for transient expression was generated using primers JM819 (5'-ACCCA-GCTTGGTACCATTGGACTACAAAGA-3') and JM820 (5'-CCTCTA-GATTACAGCTTGGAGGCATTGTCA-3'), which added an SKL peptide (TCC AAG CTG) before the stop codon. The PCR product was cloned into a pRT103 vector at the *KpnI/XbaI* sites.

Seeds were grown on 1% agar-gelled Murashige and Skoog (1962) medium, supplemented with 3% sucrose and with a pH adjusted to 5.8. Plants were grown in Petri dishes in a growth chamber maintained at $21 \pm 2^\circ\text{C}$, and a 16/8 h light/dark regime using cool white light at $70 \mu\text{mol m}^{-2} \text{sec}^{-1}$. Seedlings were used between 8 and 12 days following germination.

Flu mutant growth and re-illumination protocol

Mutant seeds were germinated on MS medium plates and either kept in total darkness for Pchlide accumulation or maintained under constant light for normal development (op den Camp *et al.*, 2003). YFP-PTS1 plants grown under identical conditions were used as controls. Dark-grown seedlings were exposed to $80 \mu\text{mol m}^{-2} \text{sec}^{-1}$ white light just prior to confocal microscopy. Time-lapse pictures of *flu* and YFP-PTS1 seedlings growing alongside each other were taken at 30 min intervals for 32 h using a Nikon Coolpix 700 digital camera (Nikon, <http://www.nikoninstruments.com>), and threaded together using Quicktime movie software (<http://www.apple.com/quicktime>).

UV irradiation

Seedlings kept in cavity slides were brought into focus on a Leica DM6000 B microscope (<http://www.leica.com>) using a 40 \times water immersion lens. A 4',6-diamidino-2-phenylindole (DAPI) filter band pass (BP)340–380 nm/dichroic 400/longpass (LP)425 nm was used to illuminate cells for the required time. Confocal imaging using Ar/HeNe lasers was started immediately following the UV illumination.

Hydrogen peroxide

Immediately before use, 30% hydrogen peroxide (approximately 8 M; Fisher Scientific, <http://www.fishersci.ca/>) was diluted to 0.80, 0.08, 0.4 and 0.008 M concentrations in distilled H₂O. Seedlings were taken directly from MS medium plates and immersed in the hydrogen peroxide for various durations ranging from 30 sec to 10 min. Subsequently, plants were removed and rinsed five times for 5 sec each with H₂O, mounted in water in a depression slide, and observed within 2 min of mounting. The duration of visualization of a cell or a region was limited to 5 min in order to limit photo-induced bleaching of chlorophyll and generation of extra ROS.

Other ROS-inducing chemicals

The hydroxyl radical-inducing mixture comprised 0.5 mM each of ascorbate and CuCl₂ in distilled water (prepared as described by

Foreman *et al.*, 2003). Xanthine/xanthine oxidase (Torres *et al.*, 2005), clofibrate (Palma *et al.*, 1991), isoproterenol (Riedel-de Haen, <http://www.riedeldehaen.de>) (Harris and Knox, 1972), Paraquat (Riedel-de Haen) (de Felipe *et al.*, 1988) or rose bengal diacetate (Knox and Dodge, 1984) (Molecular Probes, <http://www.invitrogen.com>), each prepared at 10 μM in water. Seedlings were immersed in solutions and then placed on filter paper strips in Petri dishes as described by Mathur *et al.* (2002).

Transient expression in plant cells

Transient expression of mEosFP-PTS1 in *Arabidopsis* seedling cells was performed by gold-particle coating with DNA and bombardment using a biolistic particle delivery system (Bio-Rad PDS-1000/He; <http://www.bio-rad.com/>). The manufacturer's instructions were followed for this procedure. Protein expression was assessed between 16 and 20 h after biolistic particle bombardment.

Microscopy

For live imaging, seedlings were placed in a depression slide in distilled H₂O under a glass coverslip. An upright epi-fluorescent microscope (Nikon eclipse 80i) equipped with a 40 \times Nikon Plan Apochromat lens with numerical aperture 0.95 and a 12-bit 3CCD (charge-coupled device) color digital camera (Qicam fast 1394; Qimaging, <http://www.adept.net.au/cameras/qimaging/>) was used. The chroma filter sets used were the Endow GFP-LP filter set 41018 (exciter (Ex), HQ 470/40X; Dichr, Q495LP; emitter (Em), HQ500LP), TRITC filter set 41002c (Ex, HQ545/30X; Dichr, Q570LP; Em, HQ 620/60 m) and the DAPI/Hoechst/AMCA filter set 31000V2 (Ex 350/50X; Central dichroic LP 400; Em 460/50 m). Images were captured and processed using SIMPLEPCI software (Compix Inc., <http://www.cimaging.net>). Confocal microscopy was performed using a Leica TCS-SP5 set-up with a 488 nm Ar laser and a 543 nm HeNe laser (Leica) and a Leica DM6000B microscope equipped with a 40 \times water immersion lens (numerical aperture 0.80). Images were obtained in a 1024 \times 512 pixel format in *x/y/z* and *x/y/time* dimensions, and processed using proprietary LEICA software. The time lapse between *x/y/time* scans was maintained at 1.37 sec. Sequential images had a 1 μm (*z* axis) distance between them for *x/y/z* mode acquisition. Fluorescent emission collection was at 490–510 nm for GFP, 500–522 nm for YFP, 558–596 nm for RFP and 600–680 nm for chlorophyll.

EosFP photo-conversion

Photo-conversion was performed using epi-fluorescent lighting through filter cube D (Leica. UV/violet; Ex BP 355-425/dichroic 455/LP 470 nm) using a 40 \times water immersion lens. Closing down the iris, or moving the stage so that only a small part of the cell was exposed to the beam, achieved photo-conversion of a peroxisomal subpopulation. For imaging the photo-converted probe 488 nm laser line was used at approximately 10% of its power and the weak 543 nm laser was used at 98% power.

Post-acquisition image processing

All images were cropped and processed for brightness/contrast as complete montages using Adobe Photoshop CS3 (<http://www.adobe.com>). The layer function in Photoshop was used to introduce text, regions of interest and color overlays. Images acquired using the Leica confocal microscope were processed directly using fluorescence intensity quantification tools (in various regions of interest) and the NIH ImageJ 1.40 g histogram analysis tool (Image J, <http://rsbweb.nih.gov/ij/>) and the interactive 3D surface plot plug-in. For Figure 3, P.Color5 LUT, a proprietary greyscale partitioning algorithm in the Leica TCS SP5 confocal software was used. This splits fluorescence intensity

into three equal values on a 0–255 integer scale (256 values), with blue color representing the most fluorescent regions within an image.

Calculation of peroxisome speed was based on a sample of 200 peroxisomes (10 peroxisomes each from 20 cells) per time point acquired using 10 time-lapse frames separated by 1.67 sec.

All experiments reported were replicated four times. Measurements are provided as mean value \pm standard error followed by the total number (*n*) of observed cells/organelles.

ACKNOWLEDGEMENTS

We thank Klaus Apel (Institute of Plant Sciences, ETH Zurich, Switzerland) for the *flu* mutant seeds, Jeorg Wiedenmann (University of Southampton, U.K.) for EosFP, and Daniel Johnstone for help with *Agrobacterium* transformation. Funding from the Natural Sciences and Engineering Research Council of Canada, the Canada Foundation for Innovation, the Ministry of Research and Innovation, Ontario, and the Keefer Trust, University of Guelph, is gratefully acknowledged.

SUPPORTING INFORMATION

Additional Supporting Information may be found in the online version of this article:

Figure S1. Distribution of peroxisome sizes in 20 senescent cotyledon cells from 10 seedlings.

Movie S1. Extension of peroxules in normal chlorophyll containing cells of a transgenic Arabidopsis plant expressing YFP-PTS1, which highlights peroxisomes.

Movie S2. Peroxisomes highlighted using a green to red photoconvertible EosFP-PTS1 probe were found to elongate upon H₂O₂ treatment.

Movie S3. Extension of peroxules in the vicinity of chloroplasts.

Movie S4. Co-alignment of a single elongated peroxisome with underlying ER tubules suggests a basis for its shape and peristaltic motion.

Please note: Wiley-Blackwell is not responsible for the content or functionality of any supporting information supplied by the authors. Any queries (other than missing material) should be directed to the corresponding author for the article.

REFERENCES

- op den Camp, R.G.L., Przybyla, D., Ochsenbein, C. *et al.* (2003) Rapid induction of distinct stress responses after the release of singlet oxygen in *Arabidopsis*. *Plant Cell* **15**, 2320–2332.
- Campbell, R.E., Tour, M.O., Palmer, A.E., Steinbach, P.A., Baird, G.S., Zacharias, D.A. and Tsien, R.Y. (2002) A monomeric red fluorescent protein. *Proc. Natl Acad. Sci. USA* **99**, 7877–7882.
- Cutler, S.R., Erhardt, D.W., Griffiths, J.S. and Somerville, C.R. (2000) Random GFP::cDNA fusions enable visualization of subcellular structures in cells of *Arabidopsis* at a high frequency. *Proc. Natl Acad. Sci. USA* **97**, 3718–3723.
- de Duve, C. and Baudhuin, P. (1966) Peroxisomes (microbodies and related particles). *Physiol. Rev.* **46**, 323–357.
- Fagarasanu, A., Fagarasanu, M. and Rachubinski, R.A. (2006) Maintaining peroxisome populations: a story of division and inheritance. *Annu. Rev. Cell Dev. Biol.* **223**, 321–344.
- de Felipe, M.R., Lucas, M.M. and Pozuelo, J.M. (1988) Cytochemical study of catalase and peroxidase in the mesophyll of *Lolium rigidum* plants treated with isotrocuron. *J. Plant Physiol.* **132**, 67–73.
- Finkel, T. and Holbrook, N.J. (2000) Oxidants, oxidative stress and the biology of ageing. *Nature* **408**, 239–247.
- Foreman, J., Demidchik, V., Bothwell, J.H.F. *et al.* (2003) Reactive oxygen species produced by NADPH oxidase regulate plant cell growth. *Nature* **422**, 442–446.
- Frederick, S.E., Newcomb, E.H., Vigil, E.L. and Wergin, W.P. (1968) Fine-structural characterization of plant microbodies. *Planta* **81**, 229–252.

- Frohnmeyer, H. and Staiger, D. (2003) Ultraviolet-B radiation-mediated responses in plants. Balancing damage and protection. *Plant Physiol* **133**, 1420–1428.
- Geuze, H.J., Murk, J.L., Stroobants, A.K., Griffith, J.M., Kleijmer, M.J., Koster, A.J., Verkleij, A.J., Distel, B. and Tabak, H.F. (2003) Involvement of the endoplasmic reticulum in peroxisome formation. *Mol. Biol. Cell* **14**, 2900–2907.
- Halliwell, B. and Gutteridge, J.M. (1984) Oxygen toxicity, oxygen radicals, transition metals and disease. *Biochem. J.* **219**, 1–14.
- Hanson, M.R. and Sattarzadeh, A. (2008) Dynamic morphology of plastids and stromules in angiosperm plants. *Plant Cell Environ.* **31**, 646–657.
- Harris, N. and Knox, A.D. (1972) The effect of paraquat on flax cotyledon leaves: physiological and biochemical changes. *Planta* **104**, 210–219.
- Haseloff, J., Siemering, K.R., Prasher, D.C. and Hodge, S. (1997) Removal of a cryptic intron and subcellular localization of green fluorescent protein are required to mark transgenic Arabidopsis plants brightly. *Proc. Natl Acad. Sci. USA* **94**, 2122–2127.
- Herrmann, C., Wray, J., Travers, F. and Barman, T. (1992) Effect of 2,3-butanedione monoxime on myosin and myofibrillar ATPases: an example of an uncompetitive inhibitor. *Biochemistry* **31**, 12227–12232.
- Hoepfner, D., Schildknecht, D., Braakman, L., Philippsen, P. and Tabak, H.F. (2005) Contribution of the endoplasmic reticulum to peroxisome formation. *Cell* **122**, 85–95.
- Jedd, G. and Chua, N.H. (2002) Visualization of peroxisomes in living plant cells reveals acto-myosin-dependent cytoplasmic streaming and peroxisome budding. *Plant Cell Physiol.* **43**, 384–392.
- Kim, P.K., Mullen, R.T., Schumann, U. and Lippincott-Schwartz, J. (2006) The origin and maintenance of mammalian peroxisomes involves a *de novo* PEX16-dependent pathway from the ER. *J. Cell Biol.* **173**, 521–532.
- Knox, J.P. and Dodge, A.D. (1984) Photodynamic damage to plant leaf tissue by rose bengal. *Plant Sci. Lett.* **37**, 3–7.
- Koch, A., Thiemann, M., Grabenbauer, M., Yoon, Y., McNiven, M.A. and Schrader, M. (2003) Dynamin-like protein 1 is involved in peroxisomal fission. *J. Biol. Chem.* **278**, 8597–8607.
- Kost, B., Spielhofer, P. and Chua, N.H. (1998) A GFP–mouse talin fusion protein labels plant actin filaments *in vivo* and visualizes the actin cytoskeleton in growing pollen tubes. *Plant J.* **16**, 393–401.
- Lingard, M.J. and Trelease, R.N. (2006) Five Arabidopsis peroxin 11 homologs individually promote peroxisome elongation, duplication or aggregation. *J. Cell Sci.* **119**, 1961–1972.
- Logan, D.C. (2006) The mitochondrial compartment. *J. Expt. Bot.* **57**, 1225–1243.
- Magder, S. (2006) Reactive oxygen species: toxic molecules or spark of life? *Crit. Care* **10**, 208.
- Mano, S., Nakamori, C., Hayashi, M., Kato, A., Kondo, M. and Nishimura, M. (2002) Distribution and characterization of peroxisomes in Arabidopsis by visualization with GFP: dynamic morphology and actin-dependent movement. *Plant Cell Physiol.* **43**, 331–341.
- Mano, S., Nakamori, C., Kondo, M., Hayashi, M. and Nishimura, M. (2004) An Arabidopsis dynamin-related protein, DRP3A, controls both peroxisomal and mitochondrial division. *Plant J.* **38**, 487–498.
- Mathur, J. (2007) The illuminated plant cell. *Trends Plant Sci.* **12**, 506–513.
- Mathur, J. and Chua, N.H. (2000) Microtubule stabilization leads to growth reorientation in *Arabidopsis* trichomes. *Plant Cell* **12**, 465–477.
- Mathur, J., Mathur, N. and Hulskamp, M. (2002) Simultaneous visualization of peroxisomes and cytoskeletal elements reveals actin and not microtubule-based peroxisome motility in plants. *Plant Physiol.* **128**, 1031–1045.
- Meskauskiene, R., Nater, M., Goslings, D., Kessler, F., op den Camp, R. and Apel, K. (2001) FLU: a negative regulator of chlorophyll biosynthesis in *Arabidopsis thaliana*. *Proc. Natl Acad. Sci. USA* **98**, 12826–12831.
- Mullen, R.T. and Trelease, R.N. (2006) The ER–peroxisome connection in plants: development of the ‘ER semi-autonomous peroxisome maturation and replication’ model for plant peroxisome biogenesis. *Biochim. Biophys. Acta* **1763**, 1655–1668.
- Murashige, T. and Skoog, F. (1962) A revised medium for rapid growth and bioassays with tobacco tissue cultures. *Physiol. Plant.* **15**, 473–497.
- Novikoff, P.M. and Novikoff, A.B. (1972) Peroxisomes in absorptive cells of mammalian small intestine. *J. Cell Biol.* **53**, 532–560.
- Orth, T., Reumann, S., Zhang, X., Fan, J., Wenzel, D., Quan, S. and Hu, J. (2007) The PEROXIN11 protein family controls peroxisome proliferation in Arabidopsis. *Plant Cell* **19**, 333–350.

- Palma, J.M., Garrido, M., Rodriguez-Garcia, M.I. and del Rio, L.A.** (1991) Peroxisome proliferation and oxidative stress mediated by activated oxygen species in plant peroxisomes. *Arch. Biochem. Biophys.* **287**, 68–74.
- Purdue, P.E. and Lazarow, P.B.** (2001) Peroxisome biogenesis. *Annu. Rev. Cell Dev. Biol.* **17**, 701–752.
- Reisen, D. and Hanson, M.R.** (2007) Association of six YFP–myosin XI-tail fusions with mobile plant cell organelles. *BMC Plant Biol.* **7**, 6.
- Schrader, M. and Fahimi, H.D.** (2008) The peroxisome: still a mysterious organelle. *Histochem. Cell Biol.* **129**, 421–440.
- Schrader, M., Burkhardt, J.K., Baumgart, E., Luers, G., Spring, H., Volkl, A. and Fahimi, H.D.** (1996) Interaction of microtubules with peroxisomes: tubular and spherical peroxisomes in HepG2 cells and their alterations induced by microtubule-active drugs. *Eur. J. Cell Biol.* **69**, 24–35.
- Schrader, M., Wodopia, R. and Fahimi, H.D.** (1999) Induction of tubular peroxisomes by UV irradiation and reactive oxygen species in HepG2 cells. *J. Histochem. Cytochem.* **47**, 1141–1148.
- Schrader, M., King, S.J., Stroh, T.A. and Schroer, T.A.** (2000) Real time imaging reveals a peroxisomal reticulum in living cells. *J. Cell Sci.* **113**, 3663–3671.
- Scott, I., Sparkes, I.A. and Logan, D.C.** (2007) The missing link: inter-organellar connections in mitochondria and peroxisomes? *Trends Plant Sci.* **12**, 380–381.
- Stohs, S.J. and Bagchi, D.** (1995) Oxidative mechanisms in the toxicity of metal ions. *Free Radic. Biol. Med.* **18**, 321–336.
- Tabak, H.F., Hoepfner, D., Zand, A.v.d., Geuze, H.J., Braakman, I. and Huynen, M.A.** (2006) Formation of peroxisomes: present and past. *Biochim. Biophys. Acta* **1763**, 1647–1654.
- Taira, J., Mimura, K., Yoneya, T., Hagi, A., Murakami, A. and Makino, K.** (1992) Hydroxyl radical formation by UV-irradiated epidermal cells. *J. Biochem.* **111**, 693–695.
- Thoms, S. and Erdmann, R.** (2005) Dynamin-related proteins and Pex11 proteins in peroxisome division and proliferation. *FEBS J.* **272**, 5169–5181.
- Titorenko, V.I. and Mullen, R.T.** (2006) Peroxisome biogenesis: the peroxisomal endomembrane system and the role of the ER. *J. Cell Biol.* **174**, 11–17.
- Torres, M.A., Jones, J.D.G. and Dangl, J.L.** (2005) Pathogen-induced, NADPH oxidase derived reactive oxygen intermediates suppress spread of cell death in *Arabidopsis thaliana*. *Nat. Genet.* **37**, 1130.
- Wiedenmann, J., Ivanchenko, S., Oswald, F., Schmitt, F., Röcker, C., Salih, A., Spindler, K.D. and Nienhaus, G.U.** (2004) EosFP, a fluorescent marker protein with UV inducible green-to-red fluorescence conversion. *Proc. Natl Acad. Sci. USA* **101**, 15905–15910.
- Zhang, X. and Hu, J.** (2009) Two small protein families, DYNAMIN-RELATED PROTEIN3 and FISSION1, are required for peroxisome fission in *Arabidopsis*. *Plant J.* **57**, 146–159.